INDIAN JOURNAL OF SCIENCE AND TECHNOLOGY

ORIGINAL ARTICLE

Check for updates

OPEN ACCESS

Received: 18/09/2025

Accepted: 01/11/2025

Published: 02/12/2025

Citation: Gaba J, Verma D, Sharma N, Gupta S (2025) From Deflagration to Detonation: Understanding Type Ia Supernova Explosions. Indian Journal of Science and Technology 18(44): 3468-3479. https://doi.org/10.17485/IJST/v18i44.1598

* **Corresponding author**.

shashikantgupta.astro@gmail.com

Funding: GD Goenka University (Ref. No.: R&D:07/20/04)

Competing Interests: None

Published By Indian Society for Education and Environment (iSee)

ISSN
Print: 0974-6846
Electronic: 0974-5645

From Deflagration to Detonation: Understanding Type Ia Supernova Explosions

Jagriti Gaba[1], Dinkar Verma[1], Naresh Sharma[1], Shashikant Gupta[1]*

1 Department of Basic and Applied Sciences, School of Engineering and Sciences, GD Goenka University, Gurugram, Haryana, 122103, India

Abstract

Background: Type Ia supernovae (SNe Ia) are primarily understood through Chandrasekhar mass (M_{Ch}) models; however, the pure deflagration (subsonic burning front) and pure detonation (supersonic) fail to replicate the observed distribution of ^{56}Ni and intermediate mass elements. **Objectives:** We critically review the integrated delayed detonation model (DelDetM) in light of the latest observations and numerical simulations. **Method:** This review analyzes recent developments in modeling and simulations of SNe Ia explosions, focusing on near M_{Ch} delayed detonation and sub-Chandrasekhar mass double-detonation mechanisms. The models are compared against the latest observational constraints obtained from multi-wavelength photometry and nebular phase spectroscopy. We focus on the contrast between various ignition conditions, the underlying physics of detonation triggers, and the yields of nuclear reactions. **Findings:** Pure deflagration models provide insufficient explosion energy ($\sim 0.6 - 0.8 \times 10^{51}$ erg) and leave substantial unburned C-O, while pure detonation overproduces IMEs. DelDetM provides adequate ^{56}Ni mass ($0.4 - 0.8$ M) and layered ejecta structures consistent with recent observations. 3-D simulations highlight the critical role of turbulence and flame instabilities in determining deflagration-to-detonation transition, while JWST observations provide new infrared constraints on ejecta stratification. The double-detonation model further explains the observed diversity in SNe Ia. Properly tuned DelDetM can successfully explain spectra, light curves, and nucleosynthesis yields. However, 3D simulations remain challenging due to uncertainties in the transition mechanism, excess unburned material, and imperfect chemical stratification. The competing double detonation model with a thin shell also matches nucleosynthesis yields of normal SNe Ia. Insufficient understanding of progenitor evolution and the difficulty in modeling turbulence and combustion across vast scales in multidimensional simulations have been identified as major bottlenecks. **Significance:** This article integrates the latest results from computer simulations and observations and provides a precise roadmap for future research on the physical mechanisms underlying the thermonuclear runaway in SNe Ia.

Keywords: Delayed Detonation; Type Ia Supernovae; White Dwarfs; Hydrodynamical Simulations; Nucleosynthesis; Chandrasekhar Mass; Double Detonation

1 Introduction

Type Ia supernovae (SNe Ia) are bright, energetic events resulting from the thermonuclear explosion of a carbon-oxygen (C-O) white dwarf (WD) in a binary system[1,2]. The empirical correlation between their peak brightness and the subsequent decline rate, SNe Ia serve as standardizable candles for measuring cosmic distances. Their utility in cosmology led to the discovery of the accelerated expansion of the Universe[3,4].

The classical model for standard SN Ia explosion involves the Single-Degenerate (SD) channel, in which the WD accretes matter from a non-degenerate companion. As the WD approaches the Chandrasekhar mass limit ($M_{Ch} \sim 1.4$ M)[5] at sufficiently high central pressure and temperature, nuclear burning of carbon ignites, leading to a thermonuclear runaway[6,7]. Early theoretical studies demonstrated that a pure detonation (Supersonic burning front) overproduces iron-group elements. On the other hand, a pure deflagration (subsonic burning front) fails to produce enough ^{56}Ni and unbinds the star for normal SNe Ia[8,9]. The delayed detonation model (DelDetM) was proposed to overcome the above inconsistency in which a turbulent subsonic deflagration pre-expands the WD, followed by a transition to a supersonic detonation[1,10,11]. The supersonic detonation wave propagates through lower-density matter, producing the mixture of IMEs and radioactive ^{56}Ni required to match observations[9]. The DelDetM is thus a cornerstone of the M_{Ch} explosion hypothesis[12,13]. However, deflagration to detonation transition (DDT) is a complex process which involves multi-scale physics, turbulence and propagation of combustion front in an unconfined medium and hence requires multi-dimensional simulations[13,14]. Coupled with the theoretical advancements, modern facilities like JWST provide unprecedented diagnostic power[1]. In particular, the nebular-phase spectroscopy directly probes the innermost ejecta, offering tight constraints on the explosion geometry, nuclear yields, and the mass of the exploding WD. For the sub-M_{Ch} case, the double detonation (DbDet) model and violent WD merger seem favorable[5,6,15,16].

1.1 Research Contributions

The present article contributes to the field of SNe Ia research by synthesizing recent advances in understanding the microphysical origin of detonation. We analyze models based on the Zel'dovich reactivity gradient as a viable mechanism for detonation in turbulent environments relevant to M_{Ch} explosions[13]. It provides a critical comparison of the predicted final ejecta composition in terms of the distribution of IMEs, radioactive ^{56}Ni, and stable iron-group elements across major explosion models, including M_{Ch} delayed-detonation and sub-M_{Ch} double-detonation scenarios[6]. The article also critically evaluates the consistency of current multi-dimensional explosion models (both M_{Ch} and sub-M_{Ch}) against the latest photometric and spectroscopic observational data, including the nebular phase observations, which offer unique insights into the core density and chemical stratification of the ejecta[6].

1.2 Research Gaps

Despite decades of continuous efforts, certain fundamental uncertainties remain unresolved. We list some of these important issues in this section, which justify the need for this synthesis: I. Lack of a First-Principles DDT Theory: Our current understanding of the deflagration to detonation transition is limited to computer simulations to rely on parameterized models. The fundamental physical processes that govern the transition in unconfined degenerate matter are not well understood from first principles[8,13].

II. Tensions in Observables and Chemical Stratification: Current 3D DelDetM often fails to precisely match the observational constraints, sometimes predicting an unobserved mass of unburned carbon and oxygen in the ejecta, or lacking the expected degree of chemical stratification observed through spectra. Furthermore, sub-M_{Ch} models struggle to match the full width-luminosity relation and can predict viewing-angle dependency that is broader than observed[17,18].

III. Progenitor System Ambiguity: The exact binary evolution model, i.e., Single-Degenerate vs. Double-Degenerate channel, leading to the explosion, is not definitively confirmed. This situation complicates the constraint of initial conditions, such as initial mass, accretion history, etc., needed for simulations[5,19].

IV. Discrepancies in Predicted Neutron-Rich Isotopes: There are significant differences in the distribution of iron group elements between M_{Ch} and sub-M_{Ch} models. The late time spectra, when the ejecta has expanded sufficiently, are crucial to probe the mass and distribution of these elements, as they are produced in the central region. However, inconsistencies still remain in reproducing solar abundances and observationally inferred stable nickel mass fractions through computer simulations[6].

1.3 Research Questions

Based on the research gap discussed in the previous section, we address the following central questions in the present review:

I. Under what precise physical conditions is the DDT mechanism viable and sustained in Chandrasekhar-mass WDs?

II. How do the detailed spatial distribution and relative abundance of iron group elements (IGE) differ between the delayed-detonation and double-detonation scenarios?

III. Can the multi-dimensional simulations incorporating realistic DDT criteria and progenitor environments accurately reproduce the spectroscopic and photometric diversity observed in normal SNe Ia?

IV. To what extent can the recent observations, such as nebular phase observations using JWST or the detailed line profiles of IME and IGE, be used to precisely constrain the mass and geometry of the exploding WD?

The structure of the subsequent sections of this review is as follows. We will proceed by first detailing the fundamental physics of thermonuclear combustion in degenerate matter, including deflagration, detonation, and the DDT mechanism. The current state of Chandrasekhar-mass delayed-detonation models will then be examined with a focus on their hydrodynamics and nucleosynthetic yields. Following this, a comprehensive section will explore the competing sub-Chandrasekhar mass explosion models, particularly the double-detonation channel. Finally, we will synthesize constraints derived from high-cadence and late-time observations, comparing the theoretical predictions against the most recent observational data, and concluding with a roadmap for future research directions.

2 Review Methodology

The methodology for the present review is primarily based on synthesizing information drawn directly from the pioneering work by various authors, which encompasses foundational theoretical studies, hydrodynamic simulations, and observational studies of SNe Ia.

Databases Consulted: Various reputable journals in the field of astronomy and astrophysics from important databases, such as Web of Science and SCOPUS, were thoroughly searched to collect relevant information. Most of the data used in these articles is available in various databases/catalogs, e.g., the NASA Extragalactic Database (NED), and the Open Supernova Catalog (OSC), etc.

Keywords Used in Search: Since this review focuses on the theoretical modeling of SNe Ia explosions, we include the following keywords for search through the databases: Type Ia supernova, Delayed Detonation Model, Deflagration to detonation transition, Thermonuclear supernovae, White dwarf ignition, Supernova nucleosynthesis, White dwarf, Chandrasekhar mass, Sub-Chandrasekhar mass, Double detonation, Delayed detonation, Flame propagation, Intermediate mass elements, Iron-group elements, Nuclear Statistical Equilibrium.

Year of Coverage: This review covers foundational papers that established the theoretical framework for SNe Ia explosion mechanisms, such as early work on accreting white dwarf models and triggering mechanisms from the 1980s [1,12,20,21], and the delayed-detonation model hypothesis developed in the early 1990s [10,14,17,22]. The main focus is on the substantial research conducted in the last 10 to 15 years, incorporating modern multi-dimensional simulations and detailed comparisons with the latest observations, including studies published up to the present [5,15,23].

Inclusion Criteria:

a. Explosion Mechanisms: Research articles with a focus on models detailing the physical mechanism of the thermonuclear explosion of white dwarfs [5,12,17,24] especially those involving the transition between subsonic deflagration and supersonic detonation [1,8,17,25] were included.

b. DDT/DbDet Focus: Studies rigorously investigating the constraints and consequences of the DDT in Chandrasekhar-mass models [5,8,13] and the DbDet scenario in sub-Chandrasekhar-mass models [10,24,26,27] are prioritized.

c. Model Comparison and Observables: Papers that compare hydrodynamic or radiative transfer models directly against observational constraints (e.g., light curves, spectra, nucleosynthetic yields) to validate or reject explosion scenarios [10,12,14,28] are included.

Exclusion Criteria:

a. Progenitor Population Synthesis: Studies focused solely on binary population synthesis (BPS) or progenitor statistics and rates are excluded when they do not involve the explosion mechanism; however, the implications of these scenarios are discussed in case the studies include SN Ia explosion mechanism [1].

b. Cosmological Applications: Studies which focus on empirical standardization relations for cosmological applications (like the Phillips relation) are excluded unless they explicitly derive fundamental constraints on explosion physics (e.g., nucleosynthetic masses or ejecta structures) used for direct theoretical comparison [1,25,29,30].

c. Supernova Remnants (SNRs): Studies focused primarily on the long-term evolution and morphology of SNRs are generally excluded, except where they use explosion model outputs to constrain the initial explosion dynamics and elemental distribution [31,32].

Parameters for Analysis:

The analysis presented in this review compares models across various physical parameters defining the progenitor state and ignition, and links these to the synthesized material and observable signatures. These parameters are listed below:

a. Central Density at Ignition (ρ_c): Critical for Chandrasekhar mass models, determining whether electron capture occurs, which directly influences the production of stable neutron-rich elements (e.g., stable Ni, ^{54}Fe, ^{58}Ni) [15,27,33,34].

b. DDT/Detonation Criteria: These involve (i) DDT mechanism, the criteria for initiating the detonation, such as the Zel'dovich reactivity gradient mechanism [8,13,33], turbulent mixing, or transition to the distributed burning regime [12,18]; (ii) Transition Density ρ_{DDT}, the density at which the deflagration transitions to a detonation [10,12,14,15]; and (iii) Sub-M$_{Ch}$ ignition, the Core detonation mechanism (e.g., converging shock, edge-lit, or scissors scenario).

c. Progenitor/Model Parameters: (i) White Dwarf Mass comparing outcomes from near-Chandrasekhar mass models M$_{ej}$(mass of ejecta) $\approx$ 1.37 M (solar masses) [4] versus sub-Chandrasekhar core masses (e.g., 0.6 to 1.2 M) [6,10,26]; (ii) Helium Shell Mass for DbDet models, the thickness of the accreted helium layer (e.g., 0.01, 0.05, and 0.08 M) is analyzed for its impact on explosive yields and observational features [1,10,27,35]; (iii) Progenitor Metallicity to Explore parameter space often includes variations in the initial composition, particularly C/O ratio and metallicity (e.g., solar vs. sub-solar) [1,10,14,28,30].

d. Resulting Observables and Yields: (i) Radioactive Nickel Mass ^{56}Ni: The primary determinant of peak luminosity [6,8,15,28]. Models produce typical amounts ranging from 0.3 to 1.1 M [14,33]; (ii) Light Curve Width-Luminosity Relation: Comparison of synthesized light curves (peak magnitude M$_B$, decline rate Δm$_{15}$ (B)) against the observed width-luminosity relation [1, 4, 14, 30, 31]; (iii) Stable Nickel Mass M$_{58}$Ni and Ni/Fe Ratio: Observable in nebular phase MIR spectra; used to constrain high-density burning regions and central WD mass [15,28,30]; (iv) Spectral Features and Velocities: Ejecta velocities (e.g., Si II - Si II λ6355velocity) [1,14,20,30] presence of unburnt fuel (C/O, He) [[17,30,34,36], and distribution and composition of (IME; Si, S, Ar, Ca) [10,15,17,26].

3 Overview

The analysis synthesized in this review focuses on the competing theoretical models for understanding the SNe Ia explosion mechanism. We present a contrast between the M$_{Ch}$ DDT models and the sub- M$_{Ch}$ DbDet models [1,10]. A schematic overview of the basic mechanisms of both models is presented in Figure 1, while Table 1 provides a concise comparison of their key features. The early theoretical efforts established that the accreting white dwarfs could explode via various modes, such as single detonation, double detonation, and carbon deflagration, while producing large amounts of ^{56}Ni needed to power the SNe Ia light curve [20]. Modern computer simulations, especially in three dimensions (3D), are necessary to capture the crucial microphysics such as the effects of hydrodynamical instabilities, turbulence, and asymmetry inherent in these explosions [1,5,17].

Modeling processes such as the deflagration-to-detonation transition and ignition of the WD core requires high resolution [8,27]. Although both the M$_{Ch}$ DDT and sub-M$_{Ch}$ DbDet models can reproduce the observed width-luminosity relation (WLR) [26,35], they still have shortcomings; for instance, DDT models struggle with unrealistic chemical mixing, while DbDet models face issues with spectral colors caused by helium ash [17,35].

3.1 Results and Findings

This section synthesizes the key findings concerning the explosion mechanisms and element production in SNe Ia derived from the literature, primarily comparing the M$_{Ch}$ DDT models with sub-M$_{Ch}$ DbDet models.

3.1.1. Progenitor Evolution and Ignition

The SN Ia explosion mechanism is highly dependent on the conditions established during the pre-supernova phase, specifically the initial WD mass, composition (M$_{\{C+O\}}$), and the accretion rate (M$_{dot}$) [20]. In the M$_{Ch}$ explosion, thermonuclear runaway eventually ignites carbon near the center of the WD [5,20]. The nucleosynthesis outcomes crucially depend on the central density at ignition ρ_c [5,26]. The proton to total nuclei ratio Y$_e$ is small if the central ignition density is too high, leading to overproduction of Neutron-rich nuclei (like ^{54}Cr and ^{50}Ti) [10]. The central temperature T$_c$ and the temperature distribution near the carbon ignition region depend mainly on the accretion rate (M$_{dot}$) and only slightly on other conditions like M$_{(C+O)}^{(0)}$ [20].

For lower central densities or slower deflagrations, the electron capture is also lower, which leads to a higher ratio of neutron-rich isotopes Y$_e$ [10]. Conversely, higher initial central densities lead to lower central Y$_e$ values [10].

Table 1. Comparative summary of theoretical models for SNe Ia explosions. The table outlines the evolution from pure deflagration to M_{Ch} DDT and sub-M_{Ch} DbDet models, emphasizing the transition from early parameterized frameworks to modern multidimensional, physics-rich simulations addressing persistent issues in energetics, composition, and observables

Category	Milestone Works	Current Limitations	Prospective Solutions
Pure Deflagration	W7 Model validated parameterized fast deflagration [12,20].	It is not able to produce the required energy output and elemental composition and distribution [8,15].	This model has been superseded by DDT.
M_{Ch} DDT	First 3D DDT simulations achieved realistic explosion energies [17,21].	Current 3D DDT models often show a lack of chemical stratification and excessive unburned C/O [17].	Multi-physics simulations incorporating magnetic fields and rotation (though not fully explored in sources).
	Detailed models confirm stable Ni existence from high-density burning in normal SNe Ia (e.g., SN 2021aefx) [28,37,38]	Requires high central densities ($\rho_c \geq 2 \times 10^9$ g cm^{-3}) to avoid overproduction of certain elements [5,10].	Detailed constraints on ignition density ρ_c and DDT transition density ρ_{DDT} using nucleosynthesis yields (e.g., slightly below 2.2×10^7 g cm^{-3} [10,39].
Sub-M_{Ch} DbDet	Discovery that thin helium shells <0.1M can successfully trigger core detonations [1,10,40].	Models produce spectra that are often too red due to Ti and Cr line blanketing from the helium shell ashes [35].	Employing full non-LTE radiative transfer calculations (including non-thermal leptons) to better model spectral formation and coloration [26,35,40].
	3D models demonstrate complex ignition mechanisms (converging shock, edge-lit, scissors) leading to ejecta asymmetry [26,35].	Models predict gamma-ray escape times (Δm_{40}) that are too fast, suggesting insufficient mass or low opacity/high velocities [26].	Explicitly modeling the evolution of the full binary system (including the secondary WD explosion/survival) to affect late-time ejecta structure [35,40,41].
	Strong detection of [Ne II] emission in peculiar 03fg-like SNe Ia supports the violent WD merger path [33].	Core detonation ignition is not always fully resolved in current simulations, potentially leading to numerical artifacts in the mechanism [24,26].	Focusing AMR resolution on the core ignition and shell convergence regions (e.g., resolutions $\leq$ 4 km to resolve core detonation initiation accurately [18,27].

The production of neutron-rich species depends on the metallicity of the progenitor as well; for instance, Model W70, which corresponds to zero initial metallicity, produces a smaller amount of ^{58}Ni compared to Model W7.

Detailed simulations of the pre-explosion phase indicate a single-spot ignition near the center [4]. Off-center ignition in the multi-spot explosion models, such as Model N100, does not reproduce the observed strength of nickel lines and favors delayed detonation instead [5]. A comparison of various Mch models with varying numbers of ignition spots is presented in Table 2.

Table 2. Comparison of various M_{Ch} Delayed Detonation SN explosion models based on the number of ignition points (N). These models were tested by [8] to systematically explore how the number of ignition points affects the explosion outcomes

Model	Ignition Spots	Flame Geometry	Explosion Strength	^{56}Ni Yield
N3	3	Highly asymmetric	Weakest explosion	Low ($\sim$0.3 M)
N20	20	Moderately asymmetric	Intermediate	Moderate ($\sim$0.5 M)
N100	100	Nearly symmetric	Strong explosion	High ($\sim$0.6 M)
N150	150	Very symmetric	Slightly stronger	$\sim$0.65 M

3.1.2. Sub-M_{ch} Progenitors and DbDet Ignition

Sub-M_{ch} explosion models are often termed double-detonation (DbDet) models. They are triggered by a detonation in an accreted helium shell followed by another detonation in the C-O core [5,40]. Details of the model depend on the accretion rate. For slow and intermediate accretion rates, an off-center helium detonation takes place first; however, carbon deflagration starts first for rapid accretion [20]. In case of slow accretion, the mode of ignition depends on initial WD mass as well [20].

For slow accretion rates, $\dot{M} \sim 4 \times 10^{-10}$ M yr^{-1}, helium ignition takes place prior to carbon ignition in the case of small mass WDs, while carbon ignition occurs first in high mass WDs.

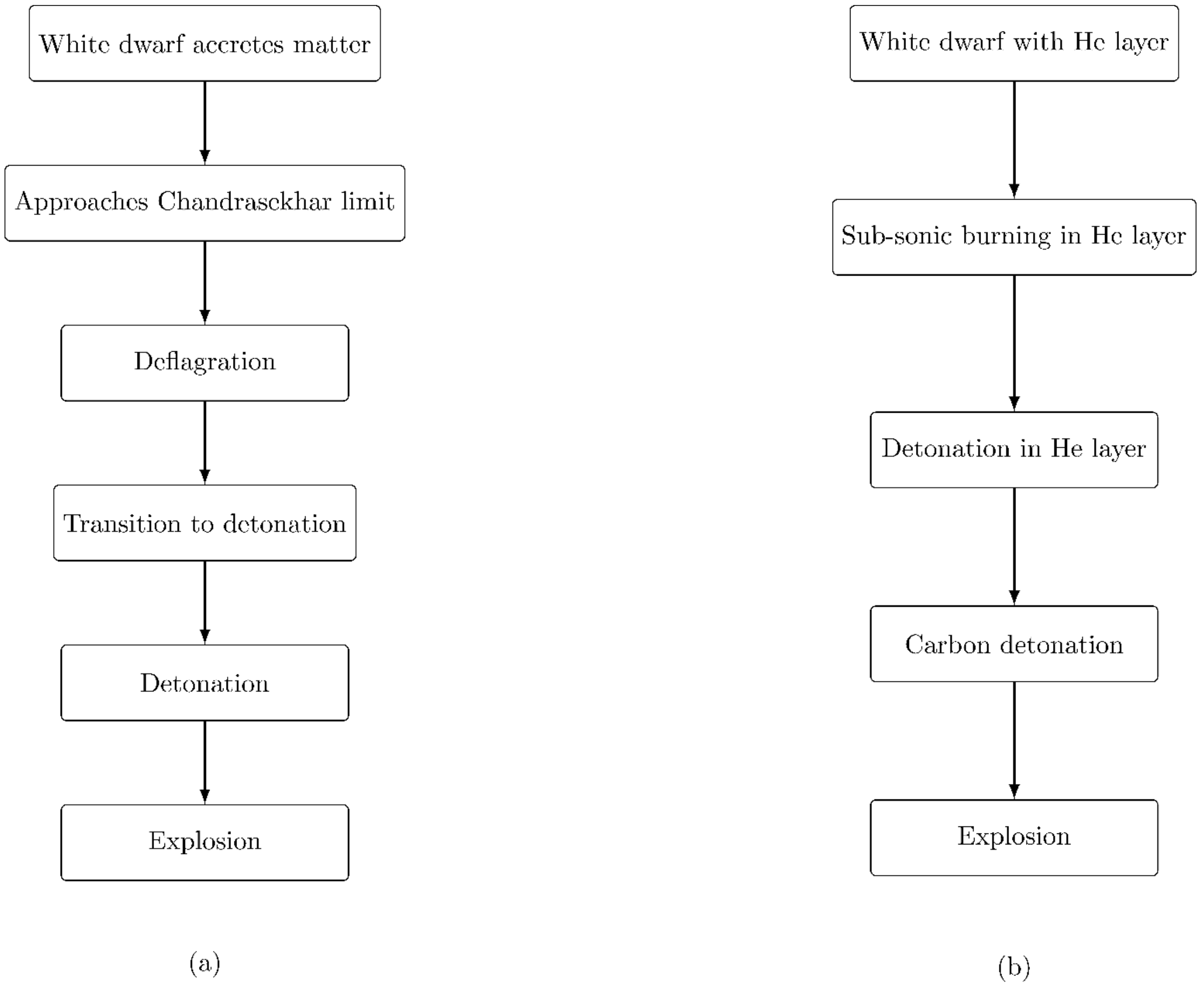

Fig 1. Schematic of Type Ia supernova explosion models: (a) Chandrasekhar-mass delayed detonation and (b) sub-Chandrasekhar double detonation scenarios

Mainly, there are three mechanisms for carbon ignition in the core after the helium shell detonation[10,26,35]. The first one is based on a converging shock in which the helium detonation drives an inward shock wave that converges near the WD center and ignites the core[10,24,26]. In the second case (edge-lit), the helium detonation directly ignites the core at the core-shell interface[10,26]. In the third case (scissors), the converging helium detonation wave ignites the carbon-enriched region between the core and the shell[26,35].

The spatial resolution and the numerical methods used in the computer simulations are the key to determining the mode of ignition[24]. Simulations with high resolution ≤ 2 km exhibit the first mechanism of converging shock. In this case, shell burning diminishes before the core ignition starts near the center[24]. Slightly coarser resolution ≥ 4 km produces the edge-lit or scissors mechanism in which the ignition is driven by mixing of hot shell material into the core and occurs at the antipodal limb[24].

3.1.3. The 3D models of the DDT scenario

Various 3D models for the DDT scenario have been proposed[17] by varying the location of the ignition point. DDT3DA is the baseline model with an ignition point near the center, while the B and C models are asymmetric in terms of ignition point geometry. A produces a higher amount of ^{56}Ni compared to the B and C models. The characteristics of the models are summarized in Table 3.

Table 3. Summary of key characteristics of representative three-dimensional Chandrasekhar-mass DDT models. The table compares variations in ignition geometry, early flame symmetry, deflagration strength, and the timing of the DDT, illustrating how initial ignition conditions influence explosion asymmetry and energetics

Model	Ignition geometry	Early flame symmetry	Deflagration strength	Time of DDT
DDT3DA	Near centre	Symmetric	Moderate	Earliest
DDT3DB	Off-centre	Mild asymmetric	Weaker	Slightly delayed
DDT3DC	Multiple ignition spots	Highly asymmetric	Strong deflagration	Latest

3.2 Chandrasekhar-Mass Deflagration and DDT Mechanisms

The thermonuclear explosion dynamics of Chandrasekhar-mass white dwarfs involve two key stages, an initial deflagration phase and then a possible transition to detonation, each determining the explosion energetics and nucleosynthetic yields of SNe Ia.

3.2.1. Chandrasekhar-Mass Deflagration

As discussed earlier, the M_{Ch} delayed-detonation model requires an initial subsonic deflagration phase followed by a transition to a supersonic detonation [(1,5,8,12,37)]. During the deflagration phase, the WD pre-expands, which is crucial for determining the final nucleosynthetic yields [(1,10)]. Characteristics of the deflagration phase are discussed below:

Flame Propagation and Instabilities: The subsonic deflagration front moving outward pushes the unburned matter, and the inward gravity causes Rayleigh-Taylor hydrodynamic instability. This causes the flame surface area to increase dramatically [(1,12,17)]. For the DDT3DA model (See Table 3), the effective burning speed remains around 0.02 c_5 until t = 0.6 s and then rises monotonically up to 0.14 c_5 at t = 1.4 s [(17)].

Pure Deflagration Limitations: Pure deflagration models (like Model W7) fail to explain normal SNe Ia because they predict too little kinetic energy, $\sim 0.6 \times 10^{51}$ erg [(1,32)] and leave large amounts of unburned C and O fuel near the star's center [(1,12,42)]. Pure deflagration models often predict ejecta that are not chemically stratified and exhibit scarce synthesis of IME [(17)].

Resolution and Convergence: Simulations with both high and medium down to $\sim 5 \times 10^5$ cm cell size resolutions indicate the convergence of results for the macroscopic parameters such as kinetic energy E_k, nuclear energy E_n, and burnt mass fraction f_b [(42)].

3.2.2. Deflagration-to-Detonation Transition (DDT)

DDT resolves the issues associated with pure deflagration [(38)]; however, the physics of DDT remains uncertain [(1,17)]. Leading mechanisms of DDT are based on the Zel'dovich reactivity gradient mechanism [(1,5,8,13)] or the onset of distributed burning when turbulence disrupts the flame sheet (occurring around $\rho \approx 10^7$ g cm^{-3}) [(12,17)].

DDT cannot be fully resolved in full-star simulations; it is often treated as a parameterized transition based on the density ρ_{DDT} at which it occurs [(12,17,42)]. DDT models with varying numbers of sparks, such as D800 with 800 ignition sparks, D20 with 20 sparks, and D5 with 5 sparks, have been tested for kinetic energy and Nuclear Statistical Equilibrium. The results indicate that the density decreases and kinetic energy increases with the reduction in the number of ignition spots [(29)].

Limitations of 3D Models: Current 3D DDT models explored show improvement over pure deflagrations but still fail to meet the basic observational constraints. The transition densities favored by 1D models $\rho_{tr} \sim 2–3 \times 10^7$ g cm^{-3}, when employed in 3D models like DDT3DA and DDT3DB produce a large remaining mass of unburned C and O ($\sim$0.4 M) [(17)]. Furthermore, these 3D DDT explosion models exhibit a lack of chemical stratification in the ejecta, which conflicts with inferences from the observations [(17)].

It has been observed that the overall properties of 3D explosions are not sensitive to variations in the initial ignition geometry (single vs. multi-point) and the precise DDT location (core, mid-altitude, or atmospheric detonation at fixed transition time) [(17)]. For instance, comparing three different DDT locations in 3D models (core, mid-altitude, atmospheric detonation) shows kinetic energy variations of only 0.15 foes and ^{56}Ni mass variations from 0.34 to 0.43 M [(17)]. This is better in contrast to 1D models, which yield a greater diversity across similar transitions [(17)].

3.3 Nucleosynthesis and Observables

The arrangement of nucleosynthetic products, especially IMEs and IGEs, informs the explosion mechanism aligns with constraints derived from ^{56}Ni masses.

3.3.1. Radioactive Nickel Yields $M^{56}Ni$

The mass of radioactive nickel ($M^{56}Ni$) is the primary determinant of peak luminosity, showing a strong correlation with the decline rate (Δm_{15} (B))[8,19]. Both M_{Ch} DDT and sub-M_{Ch} DbDet models produce substantial quantities of ^{56}Ni needed to power the light curves[8,12,20]. M_{Ch} DDT models span a wide range of $M^{56}Ni$ (e.g., 0.29 to 1.10 M in 2D models)[14]. In the 3D multi-spot DDT sequence (D800, D20, D5), the NSE mass yield varies inversely with the initial number of ignition spots, ranging from 0.638 M (D800) to 1.141 M (D5). Model D5, with few ignition spots, synthesizes more material to NSE because the detonation occurs at higher densities[29]. For sub-M_{Ch} DbDet models, $M^{56}Ni$ increases significantly as the total progenitor mass increases (e.g., above 0.9 M)[1,10]. Models with a total mass less than 0.9 M produce relatively small amounts of $M^{56}Ni$, but a significant fraction of that is often produced in the helium shell (Figure 3 in[26]). In comparison, Model M08_03 produces 0.130 M of ^{56}Ni, while Model M0905 produces 0.382 M [25]. The brightest DbDet models (e.g., 1.10 + 1.00 M two-star models) produce amounts that exceed what is expected from normal SNe Ia, aligning more with over luminous events[43].

3.3.2. Ejecta Composition and Stratification

The distribution of IME e.g., Si, S, Ca, and iron group elements IGE e.g., Fe, Ni, Cr, Ti determines the spectra and light curve features[10,17].

IME Distribution: In delayed detonation models, IME is produced during the detonation phase in low-density layers[42,44]. The ratio of Si–Ca/Fe is sensitive to the transition density (ρ_{DDT})[9]. Models with lower ρ_{DDT} (e.g., DD1 models, ρ_{DDT} = 1.7×10^7 g cm^{-3}) have larger Si–Ca/Fe ratios, which, if too high, are inconsistent with constraints derived from galactic chemical evolution[10].

Chemical Mixing and Stratification DDT: Observations require chemically stratified ejecta, with IGE confined interior to the IME layer[17]. The 3D DDT models explored in the sources generally show a lack of chemical stratification; for example, Model DDT3DA shows Fe that makes up most of the ejecta, being produced as radioactive ^{56}Ni, extending to higher velocities, while stable Ni is nearly absent from low-velocity layers[17].

C/O Remnants: Pure deflagration models leave significant C/O unburned near the center[42]. DDT models largely deplete central C/O[17] but still eject large remaining masses of unburned C/O at high velocities, exceeding observational constraints in many 3D simulations[17]. DbDet models tend to produce minimal unburnt carbon (e.g., 0.001 M for 1991bg-like events and $\leq 10^{-5}$ M for normal SNe Ia), significantly less than the $\sim$0.03 M typically found in M_{Ch} models like W7[10].

3.3.3. Spectral Signatures and Light Curve Discrepancies

He I Features (DbDet): A critical prediction of the DbDet scenario is the presence of unburnt helium in the outer ejecta[12,41,45]. Full non-LTE radiative transfer simulations confirm the prediction of a clear He I λ 10830 Å feature in the near-infrared (NIR)[40]. However, the feature's strength and persistence depend significantly on the ejecta structure: Model C23 (lower He mass, higher V) produces a feature influenced by the central Ni-rich regions, while the new model (higher He mass, lower V) shows a stronger, persistent feature dominated by the inner boundary of the He shell[45]. Both simulated features are predicted to be too strong compared to normal SNe Ia, suggesting a need for DbDet models with lower masses of ejected He[45].

Color and Line Blanketing (DbDet): Simulations of DbDet models frequently predict features inconsistent with normal SNe Ia, particularly extreme red colors[10,35]. All 3D DbDet models surveyed show extremely red colors compared to normal SNe Ia, even the lowest shell mass model (M10_02), due to strong line blanketing caused by elements like titanium (Ti II) and chromium (Cr) produced in the helium shell ashes[35]. This strong Ti II absorption would lead to classification as peculiar SNe Ia[35]. Spectral comparisons suggest the DbDet models remain promising candidates for peculiar SNe Ia but fail to match normal SNe Ia due to these coloration and spectral issues[2,35].

Asymmetry and Viewing Angle: Both M_{Ch} DDT and sub-M_{Ch} DbDet models exhibit ejecta asymmetries, leading to viewing-angle dependence in observables[6,14,26,35]. In 3D DbDet models, the U and B band light curves show an extremely strong viewing-angle dependence[35]. The predicted distribution of values on the width-luminosity relation is much broader than the spread shown by observational data[14,26,35]. For instance, in Model M10_10 (edge-lit), the brightest line of sight is viewing toward the northern pole (where ^{56}Ni is nearest the surface), while in Models M08_03 and M10_05 (converging shock/scissors), the brightest line of sight is toward the southern pole[26].

Gamma-ray Escape Time (Δm_{40}): Constraints related to the light curve decline rate for longer durations, like Δm_{40} and gamma-ray escape time (t_0), suggest a few common problems for both M_{Ch} DDT and sub-M_{Ch} DbDet models[26]. Sub-M_{Ch} DbDet models are systematically offset from the observed correlation between Δm_{15}(bol) and Δm_{40}(bol), predicting a decline that is too fast (Δm_{40} (bol) is lower) compared to observations[18,26]. This indicates very low opacity, suggesting that either the ejecta mass is too low, or the velocities are too high[26]. The Two Expl model, in which both the WDs detonate, results in a total ejecta mass significantly high ($\sim$1.75 M). On the other hand, the ejecta mass in the One Expl model, in which only one of the

WDs detonates, is much smaller (1.09 M)[18]. This difference leads to a significantly longer gamma-ray escape time (t_0) in Two Expl compared to One Expl (Figure 5 in[18]), suggesting a potential solution path for the Δm_{40} discrepancy[18].

4 Conclusion

This review integrates constraints derived from recent high-fidelity nebular and near-infrared (NIR) observations with the predictions of the latest M_{Ch} DDT and sub-M_{Ch} DbDet simulations. The analysis presented here offers new constraints on explosion physics that go beyond historical comparisons with the Phillips relation and photospheric spectra. We summarize the main findings below.

Comprehensive Summary: The M_{Ch} DDT model produces the amount of kinetic energy of the explosion and the radioactive ^{56}Ni that matches the observations and hence remains the primary theoretical model for explaining the SNe Ia explosion[1,8,12]. In this model, the WD expands initially with a subsonic deflagration followed by a transition to a supersonic detonation[12,14]. The model successfully produces the appropriate amount of high-velocity intermediate-mass elements and also resolves the issue of unburned matter near the center, thus removing the major deficiencies of the deflagration model[1,5,8].

Detailed modeling of individual transient events, such as the under-luminous events like SN 2022xkq, favors the off-center delayed-detonation of a near-M_{Ch} WD with high central density[5]. This model is well supported by the presence of electron-capture elements in their nebular spectra, which requires high-density burning regions found in massive WDs[27,28].

However, modern three-dimensional DDT simulations operating in the density range ρtr $\sim$ 1- 4 $\times$ 10^7 g cm^{-3} still suffer from fundamental issues[17], as their predictions often lack chemical stratification and show ejection of excessive mass of unburned carbon and oxygen (C/O)[1,17]. Moreover, 1D M_{Ch} models fail to account for the buoyant rise of deflagration ash, leading to an inversion of detonation and deflagration products[6] and hence are not successful in explaining the SNe Ia explosion.

The detection of stable Ni in nebular spectra of SNe Ia using JWST strongly supports a high WD mass progenitor ($\geq$ 1.2 M) that undergoes nuclear burning[5,39,43] at high density. The observations support an off-center delayed detonation.

4.1 Limitations and Challenges:

The scope of this review is limited to the comparison between M_{Ch} delayed-detonation and sub-M_{Ch} double-detonation models. Despite decades of research, several fundamental knowledge gaps persist regarding the M_{Ch} DDT scenario:

1. The Precise DDT Mechanism: The physics behind the deflagration-to-detonation transition remains unresolved[1,8,12,13,17]. While theoretical concepts such as the Zel'dovich reactivity gradient mechanism or distributed nuclear burning have been proposed, a definitive, self-consistent physical model for DDT initiation in the unconfined medium of a white dwarf is still lacking[1,8,13]. This limitation necessitates treating the DDT density (ρ_{DDT}) as an artificial parameter in large-scale simulations[5,8,28]. Progenitor System Details: The exact nature of the companion star in the single-degenerate scenario and the details of mass accretion leading to a near-M_{Ch} explosion remain unclear[6,12,42]. Modeling this accretion phase is highly challenging due to uncertainties in parameters such as the retention efficiency of accreted material and the critical accretion rates required for stable nuclear burning[1,12]. The ignition spot geometry, that is, whether ignition occurs at a single spot or multiple spots within the white dwarf core, also strongly influences the subsequent explosion and is not yet determined from first principles[5,8].
2. Chemical Stratification in 3D: Although current three-dimensional DDT simulations produce satisfactory nucleosynthetic yields, they fail to reproduce the chemically stratified ejecta observed in real events, and thus remain inconsistent with observations[17,22].

4.2 Roadmap for Future Work:

Future work must address the convergence, fidelity, and observational testing of M_{Ch} DDT models:

1. Develop Physically Consistent Subgrid-Scale (SGS) Models: Future simulations should focus on developing and rigorously testing SGS models for DDT that are consistent with physical constraints (e.g., turbulent velocities and fractal flame surfaces) and independent of numerical resolution, moving beyond simple density parameterizations[8].
2. Achieve Full 3D NLTE Radiative Transfer: It is crucial to proceed with full three-dimensional non-LTE (NLTE) radiative transfer simulations coupled to 3D hydrodynamic DDT outputs[1,6,12,14,28]. This is necessary to correctly map the inherently asymmetric ejecta structure, including the high-velocity deflagration ash, to synthetic observables, particularly for nebular spectra, and to avoid the fundamentally unphysical results of 1D models[6].

3. Targeted Observational Constraints: Specific observational campaigns, especially using JWST/MIRI, should be prioritized to obtain high-resolution late-time MIR spectra of a larger sample of normal and transitional SNe Ia [6,28,40]. These observations can definitively test the model predictions regarding the width and distribution of stable Ni and Fe lines, providing firm constraints on core burning physics and mixing.
4. Upcoming Missions: The Large Synoptic Survey Telescope (LSST) is an ambitious upcoming survey designed to probe dark energy, dark matter, and transient objects. It will begin observations in 2025 [46] to provide precise information about the light curve shape and the intrinsic peak luminosity of SNe Ia, thereby improving our understanding of the physics of SNe Ia and their calibration for cosmological applications [46]. Furthermore, UV observations from the upcoming UVIa mission will offer additional insights to enhance our understanding of the explosion mechanisms of SNe Ia [47].

5 Nomenclature

Table 4. Definitions of the specialized terms are presented here

Abbreviation	Full Form
SNe Ia	Type Ia Supernovae
WD	White Dwarf
C-O	Carbon-Oxygen
M_{Ch}	Chandershekhar mass
Sub- M_{Ch}	Sub-Chandershekhar mass
DelDetM	Delayed detonation model
DDT	Deflagration to detonation transition
DbDet	Double detonation
IGE	Iron group elements
IME	Intermediate mass elements
NSE	Nuclear statistical equilibrium
NED	NASA extragalactic database
OSC	Open supernova catalog
ρ_{DDT}	Transition density
M_{ej}	Mass of ejecta
M	Solar masses
M_B	Peak Bolometric Magnitude
Δm_{15} (B)	Decline rate in B band
WLR	Width-luminosity relation
SGS	Subgrid-Scale
SD	Single-Degenerate

6 Acknowledgment

Shashikant Gupta gratefully acknowledges GD Goenka University for providing the seed grant (Ref. No.: R&D: 07/20/04) that supported the present work.

References

1) Ruiter AJ, Seitenzahl IR. Type Ia supernova progenitors: a contemporary view of a long-standing puzzle;vol. 33. Springer Berlin Heidelberg. 2025. https://doi.org/10.48550/arXiv.2412.01766.
2) Hillebrandt W, Kromer M, Röpke FK, Ruiter AJ. Towards an understanding of Type Ia supernovae from a synthesis of theory and observations. *Frontiers of Physics*. 2013 Apr;8(2):116–143. https://doi.org/10.1007/s11467-013-0303-2.
3) Perlmutter S, Aldering G, Valle MD, Deustua S, Ellis RS, Fabbro S, et al. Discovery of a supernova explosion at half the age of the Universe. *Nature*. 1998 Jan;391(6662):51–54. https://doi.org/10.1038/34124.
4) Riess AG, Filippenko AV, Challis P, Clocchiatti A, Diercks A, Garnavich PM, et al. Observational evidence from supernovae for an accelerating universe and a cosmological constant. *The Astronomical Journal*. 1998 Sep;116(3):1009. https://doi.org/10.1086/300499.

5) DerKacy JM, Ashall C, Hoeflich P, Baron E, Shahbandeh M, Shappee BJ, et al. JWST MIRI/Medium Resolution Spectrograph (MRS) observations and spectral models of the underluminous Type Ia supernova 2022xkq. *The Astrophysical Journal*. 2024;961(2):187. https://doi.org/10.3847/1538-4357/ad0b7b.
6) Pakmor R, Seitenzahl IR, Ruiter AJ, Sim SA, Röpke FK, Taubenberger S, et al. Type Ia supernova explosion models are inherently multidimensional. *Astronomy & Astrophysics*. 2024 Jun;686:A227. https://doi.org/10.1051/0004-6361/202449637.
7) Johnson JA. Populating the periodic table: Nucleosynthesis of the elements. *Science*. 2019 Feb;363(6426):474–478. https://doi.org/10.1126/science.aau9540.
8) Ciaraldi-Schoolmann F, Seitenzahl IR, Röpke FK. A subgrid-scale model for deflagration-to-detonation transitions in Type Ia supernova explosion simulations: Numerical implementation. *Astronomy & Astrophysics*. 2013 Nov;559:A117. https://doi.org/10.1051/0004-6361/201321480.
9) Brooker E, Plewa T, Fenn D. SN Ia DDT Explosions Powered by the Zeldovich Reactivity Gradient Mechanism. *Monthly Notices of the Royal Astronomical Society*. 2020 Aug. https://doi.org/10.48550/arXiv.2008.05010.
10) Polin A, Nugent P, Kasen D. Observational predictions for sub-Chandrasekhar mass explosions: Further evidence for multiple progenitor systems for Type Ia supernovae. *The Astrophysical Journal*. 2019;873(1):84. https://doi.org/10.3847/1538-4357/aafb6a.
11) Khokhlov AM. Delayed detonation model for type IA supernovae. *Astronomy and Astrophysics*. 1991 May;245(1):114–128. https://ui.adsabs.harvard.edu/abs/1991A%26A...245..114K/abstract.
12) Hillebrandt W, Niemeyer JC. Type Ia supernova explosion models. *Annual Review of Astronomy & Astrophysics*. 2000 Sep;38(1):191–230. https://doi.org/10.48550/arXiv.astro-ph/0006305.
13) Brooker E, Plewa T, Fenn D. Type Ia supernovae deflagration-to-detonation transition explosions powered by the Zel'dovich reactivity gradient mechanism. *Monthly Notices of the Royal Astronomical Society: Letters*. 2021 Feb;501(1):L23–L27. https://doi.org/10.1093/mnrasl/slaa141.
14) Blondin S, Kasen D, Röpke FK, Kirshner RP, Mandel KS. Confronting 2D delayed-detonation models with light curves and spectra of Type Ia supernovae. *Monthly Notices of the Royal Astronomical Society*. 2011 Oct;417(2):1280–1302. https://doi.org/10.1111/j.1365-2966.2011.19345.x.
15) Siebert MR, Kwok LA, Johansson J, Jha SW, Blondin S, Dessart L, et al. Ground-based and JWST observations of SN 2022pul. I. Unusual signatures of carbon, oxygen, and circumstellar interaction in a peculiar type Ia supernova. *The Astrophysical Journal*. 2024 Jan;960(1):88. https://doi.org/10.3847/1538-4357/ad0975.
16) Ghosh A, Kushnir D. Confronting double-detonation sub-Chandrasekhar models with the low-luminosity suppression of Type Ia supernovae. *Monthly Notices of the Royal Astronomical Society*. 2019;p. 1–7. https://doi.org/10.1093/mnras/stac1846.
17) Bravo E, Garcia-Senz D. A three-dimensional picture of the delayed-detonation model of type Ia supernovae. *Astronomy & Astrophysics*. 2008 Feb;478(3):843–853. https://ui.adsabs.harvard.edu/link_gateway/2008A&A...478..843B/doi:10.1051/0004-6361:20078424.
18) Pakmor R, Callan FP, Collins CE, de Mink SE, Holas A, Kerzendorf WE, et al. On the fate of the secondary white dwarf in double-degenerate double-detonation Type Ia supernovae. *Monthly Notices of the Royal Astronomical Society*. 2022;517(4):5260–5271. https://doi.org/10.1093/mnras/stac3107.
19) Soker N. A double-degenerate scenario with a merger to explosion delay time to explain Type Ia supernova SN 2020aeuh. *Research in Astronomy and Astrophysics*. 2025 Jul. https://doi.org/10.48550/arXiv.2507.16757.
20) Nomoto K. Accreting white dwarf models for type I supernovae. I-Presupernova evolution and triggering mechanisms. *The Astrophysical Journal, Part 1*. 1982 Feb;253:798–810. https://doi.org/10.1086/159682.
21) Arnett WD. On the theory of Type I supernovae. *The Astrophysical Journal, Part 2 - Letters to the Editor*. 1979 May;230:L37–L40. https://doi.org/10.1086/182957.
22) Kasen D, Röpke FK, Woosley SE. The diversity of type Ia supernovae from broken symmetries. *Nature*. 2009 Aug;460(7257):869–872. https://doi.org/10.1038/nature08256.
23) Zingale M, Chen Z, Rasmussen M, Polin A, Katz M, Clark AS, et al. Sensitivity of simulations of double-detonation Type Ia supernovae to integration methodology. *The Astrophysical Journal*. 2024;966(2):150. https://doi.org/10.3847/1538-4357/ad3441.
24) Rivas F, Harris JA, Hix WR, Messer OEB. The impact of resolution on double-detonation models for Type Ia supernovae. *The Astrophysical Journal*. 2022 Sep;937(1):2. https://doi.org/10.3847/1538-4357/ac8b06.
25) Harvey L, Maguire K, Magee MR, Bulla M, Dhawan S, Schulze S, et al. Early-time spectroscopic modelling of the transitional Type Ia supernova 2021rhu with TARDIS. *Monthly Notices of the Royal Astronomical Society*. 2023 Jul;522(3):4444–4467. https://doi.org/10.1093/mnras/stad1226.
26) Gronow S, Collins CE, Sim SA, Röpke FK. Double detonations of sub-Chandrasekhar mass CO white dwarfs: Can differently core and He shell masses explain variations of Type Ia supernovae? *Astronomy & Astrophysics*. 2021 Feb. https://doi.org/10.1051/0004-6361/202039954.
27) Liu ZW, Röpke FK, Zeng Y, Heger A. Observational signatures of the surviving donor star in the double-detonation model of Type Ia supernovae. *Astronomy & Astrophysics*. 2021 Oct;654:A103. https://doi.org/10.1051/0004-6361/202141518.
28) DerKacy J, Ashall C, Hoeflich P, Baron E, Shappee B, Baade D, et al. JWST low-resolution MIRI spectral observations of SN 2021aefx: high-density burning in a type Ia supernova. *The Astrophysical Journal Letters*. 2023 Feb;945(1):L2. https://doi.org/10.3847/2041-8213/acb8a8.
29) Mazzali PA, Röpke FK, Benetti S, Hillebrandt W. A common explosion mechanism for type Ia supernovae. *Science*. 2007 Feb;315(5813):825–828. https://doi.org/10.1126/SCIENCE.1136259.
30) Kawabata M, Maeda K, Yamanaka M, Nakaoka T, Kawabata KS, Adachi R, et al. SN 2019ein: New Insights into the Similarities and Diversity among High-velocity Type Ia Supernovae. *The Astrophysical Journal*. 2020 Apr;893(2):143. https://doi.org/10.3847/1538-4357/ab8236.
31) Ferrand G, Warren DC, Ono M, Nagataki S, Röpke FK, Seitenzahl IR. From supernova-to-supernova remnant: The three-dimensional imprint of a thermonuclear explosion. *The Astrophysical Journal*. 2019 Jun;877(2):136. https://doi.org/10.3847/1538-4357/ab1a3d.
32) Ferrand G, Warren DC, Ono M, Nagataki S, Röpke FK, Seitenzahl IR, et al. From supernova-to-supernova remnant: Comparison of thermonuclear explosion models. *The Astrophysical Journal*. 2021;906(2):93. https://doi.org/10.3847/1538-4357/abc951.
33) Kwok LA, Siebert MR, Johansson J, Jha SW, Blondin S, Dessart L, et al. Ground-based and JWST Observations of SN 2022pul. II. Evidence from nebular spectroscopy for a violent merger in a peculiar type Ia supernova. *The Astrophysical Journal*. 2024 Apr;966(1):135. https://doi.org/10.3847/1538-4357/ad2c0d.
34) Hoeflich P, Yang Y, Baade D, Cikota A, Maund JR, Mishra D, et al. The core normal Type Ia supernova 2019np – an overall spherical explosion with an aspherical surface layer and an aspherical 56Ni core. *Monthly Notices of the Royal Astronomical Society*. 2023 Mar;520(1):560–582. https://doi.org/10.1093/mnras/stad172.
35) Collins CE, Gronow S, Sim SA, Röpke FK. Double detonations: Variations in Type Ia supernovae due to different core and He shell masses II. Synthetic observables. *Monthly Notices of the Royal Astronomical Society*. 2022;517(4):5289–5302. https://doi.org/10.1093/mnras/stac2665.
36) Liu J, Wang X, Filippenko AV, Brink TG, Yang Y, Zheng W, et al. Implications for the explosion mechanism of Type Ia supernovae from their late-time spectra. *Monthly Notices of the Royal Astronomical Society*. 2023 Nov;526(1):1268–1286. https://doi.org/10.1093/mnras/stad2851.

37) Arnett D, Livne E. The delayed-detonation model of a type IA supernovae. 1: The deflagration phase. *The Astrophysical Journal, Part 1*. 1994 May;427(1):315–329. https://doi.org/10.1086/174142.
38) Kwok LA, Jha SW, Temim T, Fox OD, Larison C, Camacho-Neves Y, et al. A JWST near-and mid-infrared nebular spectrum of the type Ia supernova 2021aefx. *The Astrophysical Journal Letters*. 2023 Feb;944(1):L3. https://iopscience.iop.org/article/10.3847/2041-8213/acb4ec.
39) Khokhlov AM, Oran ES, Wheeler JC. Deflagration-to-detonation transition in thermonuclear supernovae. *The Astrophysical Journal*. 1997 Apr;478(2):678. https://doi.org/10.1086/303815.
40) Collins CE, Sim SA, Shingles LJ, Gronow S, Röpke FK, Pakmor R, et al. Helium as a signature of the double detonation in Type Ia supernovae. *Monthly Notices of the Royal Astronomical Society*. 2023;524(3):4447–4454. https://academic.oup.com/mnras/article/524/3/4447/7226708.
41) Hoeflich P, Ashall C, Bose S, Baron E, Stritzinger MD, Davis S, et al. Measuring an Off-center Detonation through Infrared Line Profiles: The Peculiar Type Ia Supernova SN 2020qxp/ASASSN-20jq. *The Astrophysical Journal*. 2021 Nov;922(2):186. Available from: https://iopscience.iop.org/article/10.3847/1538-4357/ac250d.
42) Gamezo VN, Khokhlov AM, Oran ES, Chtchelkanova AY, Rosenberg RO. Thermonuclear supernovae: Simulations of the deflagration stage and their implications. *Science*. 2003 Jan;299(5603):77–81. https://doi.org/10.1126/science.1078129.
43) Boos SJ, Townsley DM, Shen KJ. Type Ia supernovae can arise from the detonations of both stars in a double degenerate binary. *The Astrophysical Journal*. 2024 Sep;972(2):200. https://doi.org/10.3847/1538-4357/ad5da2.
44) Mori K, Famiano MA, Kajino T, Suzuki T, Garnavich PM, Mathews GJ, et al. Nucleosynthesis constraints on the explosion mechanism for type Ia supernovae. *The Astrophysical Journal*. 2018 Aug;863(2):176. https://iopscience.iop.org/article/10.3847/1538-4357/aad233.
45) Callan FP, Collins CE, Sim SA, Shingles LJ, Pakmor R, Srivastav S, et al. Exploring the range of impacts of helium in the spectra of double detonation models for Type Ia supernovae. *Monthly Notices of the Royal Astronomical Society*. 2024 Aug. http://arxiv.org/abs/2408.03048.
46) Ž Ivezić, Kahn SM, Tyson JA, Abel B, Acosta E, Allsman R, et al. LSST: from science drivers to reference design and anticipated data products. *The Astrophysical Journal*. 2019 Mar;873(2):111. https://doi.org/10.3847/1538-4357/ab042c.
47) Hoadley K, McCully C, Kyne G, Aguirre FC, Andrews M, Basset C, et al. The Ultraviolet Type Ia Supernova CubeSat (UVIa): Science Motivation & Mission Concept. *arXiv preprint*. 2025 Feb. https://doi.org/10.48550/arXiv.2502.11957.